

NUMERICAL SIMULATION OF FLOW AND HEAT TRANSFER AROUND THREE CYLINDERS IN TRIANGULAR ARRANGEMENT

Luis Fernando Posada Cuadro, luis.cuadro@acad.pucrs.br

Marco Carrilho Diniz, marco.diniz@acad.pucrs.br

Jorge Hugo Silvestrini, jorgehs@pucrs.br

Faculdade de Engenharia, Pontifícia Universidade Católica do Rio Grande do Sul
Av. Ipiranga, 6681, Porto Alegre, RS
90619-900, Brasil

Abstract. *This work presents results from two-dimensional numerical simulations of incompressible flow and heat transfer around three cylinders. The distance between the cylinder centres is maintained constant equal to two diameters. Six arrangements are considered depending on the angle of attack α . The simulations were performed using a computational code that solves numerically the Navier-Stokes, continuity and energy equations. The numerical method is based on a sixth-order compact finite-difference scheme to compute the spatial derivatives and a third-order low-storage Runge-Kutta method for time integration. The cylinders are modelled using an immersed boundary method. For all the simulations, the Reynolds number is equal to $Re=300$ while the Prandtl number is $Pr=1$. Velocity, vorticity and temperature fields are examined for each configuration. Using momentum and energy integral balances around suitable control volumes, the drag and lift coefficients, and Nusselt numbers are computed. Results indicate that angle of attack variation affects significantly the vorticity and temperature fields. The maximum mean Nusselt number is found for the configuration $\alpha = 60^\circ$, which also corresponds to the maximum mean drag coefficient. The vortex shedding mechanism, analysed through the power density spectrum of velocity fields, denote that depending on the configuration, different Strouhal numbers corresponding to peak values of kinetic energy may be found. The $\alpha = 60^\circ$ case is also characterized by the maxima values of Reynolds stress at the near field wake.*

Keywords: *heat transfer, vortex shedding, Nusselt number, drag and lift coefficient, circular cylinder*

1. INTRODUCTION

Fluid flow with heat transfer around cylinders is a typical configuration of many important industrial processes and real life conditions such as fluid filtration in biological systems, tubular heat exchangers, nuclear reactors, etc. Despite the fact that some characteristics of these flows are already known, the interference among cylinders, the resulting vortex shedding model and the influence on heat transfer rate are less understood. Therefore is necessary to analyse the detailed dynamics of vorticity and temperature fields to improve our knowledge of non stationary convective heat transfer and fluid flow, for optimizing design of heat exchangers.

Flow involving cylinders has been experimentally and numerically studied, particularly the flow around a single cylinder (Williamson, 1996; Lamballais and Silvestrini, 2002), side-by-side configurations (Bearman and Wadock, 1973; Ribeiro *et al.*, 2002; Wang and Zhou, 2004; to mention few of them) and in tube arrays (Polak and Weaver, 1995; Lam and Zou, 2009). These studies show that the vortex shedding is related to the gap between the cylinders and has different characteristics depending on the flow. In particular, in the side-by-side arrangement, the prominent feature is the bistable characteristic of the flow for relative lows gaps.

The three cylinders model in a triangular arrangement is a classical configuration in a tube bank of a heat exchanger. Researches for this model seem to be less numerous than for other configurations, especially with heat transfer. Lam and Cheung (1988) describes the flow around a three cylinders triangular configuration at different angles of incidence and spacing ratio. Chou and Chao (1991) investigated experimentally the behaviour of the flow around three cylinder arrangement with different longitudinal and vertical separations at low Reynolds number. Igarashi (1993) carried out experimental measures to predict aerodynamic forces in a three cylinders configuration arranged in line. Wu *et al.* (2006) investigated numerically the effect of transient mixed convection interaction between three cylinders arranged in triangular configuration for different gaps.

In this paper, the two-dimensional flow and heat transfer around an equilateral arrangement of three identical cylinders is analysed using numerical simulation. Focus is centred on the influence exerted by a solid rotation of the cylinders arrangement on the flow and heat transfer characteristics. In the next section, the governing equations are presented along with the immersed boundary methods used to describe the fluid flow and heat transfer around obstacles in Cartesian grids. In section 3, the domain configuration is presented along with the corresponding boundary conditions and the numerical methods used. Finally, the main results about instantaneous temperature fields, aerodynamics forces, Nusselt numbers, characteristic frequencies of vortex shedding and mean and turbulent statistics are presented and discussed.

2. MATHEMATICAL MODEL

The behaviour of incompressible flows with heat transfer can be simulated solving the Navier-Stokes and the energy equations. In this work, the constant-property non-dimensional conservation equations, written in vectorial notation, are used in the form:

$$\vec{\nabla} \cdot \vec{u} = 0, \quad (1)$$

$$\frac{\partial \vec{u}}{\partial t} + \vec{\omega} \times \vec{u} = -\vec{\nabla} p + \frac{1}{Re} \nabla^2 \vec{u} + \vec{f}, \quad (2)$$

$$\frac{\partial \theta}{\partial t} + (\vec{u} \cdot \vec{\nabla}) \theta = \frac{1}{RePr} \nabla^2 \theta + g. \quad (3)$$

In Eqs. (1-3) \vec{u} is the velocity field, p the modified pressure field, \vec{f} the external forces, $\vec{\omega}$ the vorticity field given by $\vec{\omega} = \vec{\nabla} \times \vec{u}$, θ the temperature field, g a source/sink term, Re the Reynolds number, and Pr the Prandtl number. The equations are normalized using the inlet velocity U_∞ , the cylinder diameter D , the temperatures T_c (cylinder temperature), and T_∞ (free-stream temperature). The temperature field θ is defined as

$$\theta(\vec{x}, t) = \frac{T(\vec{x}, t) - T_c}{T_\infty - T_c}. \quad (4)$$

The immersed boundary method is used to model the cylinder influence on fluid flow and heat transfer. Different formulations have been proposed (Lamballais and Silvestrini, 2002; Linnick and Fasel, 2003). In this work, the feedback force methodology proposed by Goldstein *et al.* (1993) is adopted. With this methodology, the force term in Eq. (2) can be described as a harmonic oscillator given by:

$$\vec{f}(\vec{x}_s, t) = \alpha_f \int_0^t \vec{u}(\vec{x}_s, t) dt + \beta_f \vec{u}(\vec{x}_s, t), \quad (5)$$

where \vec{x}_s represents the immersed boundary. Similarly, the term g added in Eq. (3) represents the virtual heat source/sink term such that the desired cylinder temperature or heat flux at the wall is obtained. For an isothermal cylinder, it can be done by the equation:

$$g(\vec{x}_s, t) = \alpha_\theta \int_0^t \theta(\vec{x}_s, t) dt + \beta_\theta \theta(\vec{x}_s, t). \quad (6)$$

In Eqs. (5-6), the constants α_f , α_θ , β_f and β_θ are negatives and characterize the oscillation frequency and the damping of the dynamical system.

3. FLOW CONFIGURATION AND NUMERICAL METHOD

Eqs. (1-3) are solved in the two-dimensional domain configuration shown in Fig. 1. The boundary conditions are also specified in the figure. In the x -direction, inlet/outlet conditions are imposed. The inlet condition is defined with a constant free-stream velocity and temperature, while the outlet condition is obtained through the resolution of a simplified convection equation (shown in the figure). The approximated convective velocity of the vortices at the outlet (U_b), corresponds to the mean convective velocity of Kármán's vortices. In the y -direction, free-slip conditions are considered while, at the obstacles, Eqs. (5,6) provide no-slip and constant wall temperature conditions. In Fig. 1, the longitudinal and transversal separations between cylinders S_H and S_V , the location of the triangular arrangement centre x_c and y_c and the angle characterizing the cylinders configuration α are also introduced.

Eqs (1-3), along with the boundary conditions specified, are solved numerically using the `incompact3d` computational code (Lardeau *et al.*, 2002). This code is based on high performance numerical methods such as the sixth-order finite-difference scheme, used to compute the spatial derivatives, and a third-order low-storage Runge-Kutta method (Williamson, 1985) that performs time integration. The continuity equation (Eq. 1) is ensured with a fractional step method via resolution of a Poisson equation for the pressure. The small time step, the high number of grid nodes used and the numerical methods employed result in a very accurate simulation that may be considered a two-dimensional Direct Numerical Simulation (2D DNS). The `incompact3d` numerical code has been intensively used in different configurations associated with the flow around a single cylinder (see for instance, Lamballais and Silvestrini, 2002; Vitola *et al.* 2004), passive control of vortex shedding using plates, also for a single cylinder (Ribeiro *et al.*, 2004); side-by-side cylinders configuration (Ribeiro *et al.*, 2002), and on the flow around aerodynamical obstacles (Ortega *et al.*, 2007). First results of `incompact3d` computational code of fluid flow with heat transfer around cylinders, were reported by Giacomello *et al.*, (2006) and Hoffmann (2007).

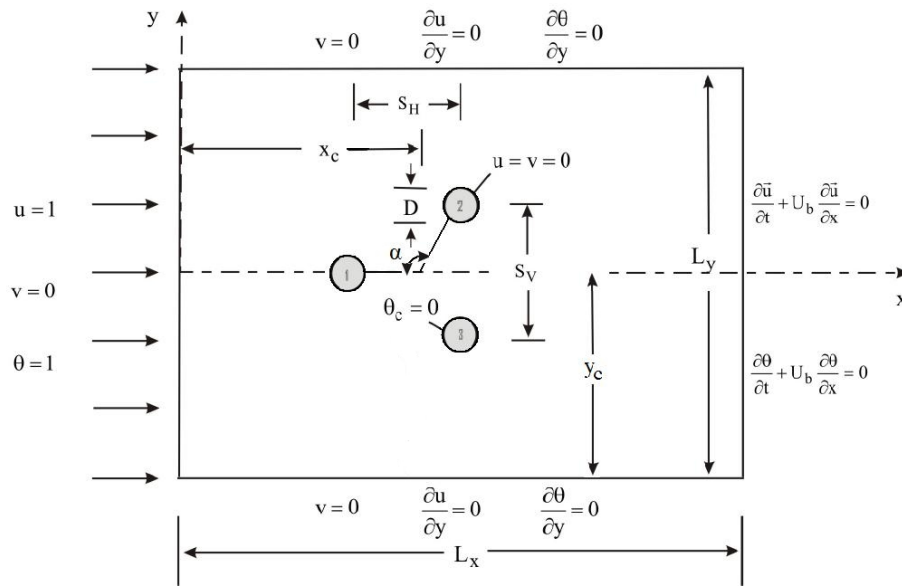


Figure 1. Domain configuration and boundary conditions.

Table 1 presents a comparison between Hoffman (2007) results, obtained through *incompact3d* computational code, and other published results on heat and fluid flow around a single cylinder. In this table, the mean Nusselt number corresponding to the heat transfer between the fluid flow and a single cylinder for $Re = 100, 200,$ and 300 and $Pr = 0.715$ and 1 , is presented. The agreement among the results is fairly good despite differences in the employed methods. This differences are due to variation of blockage ratio, grid resolution, numerical method and immersed boundary method (if used). A typical time serie of Nusselt number, denoting the instationary heat transfer for $Pe = Re.Pr = 300$, (Pe is the Peclet number) is shown in Fig. 2.

Pr	Re	1	2	3	4	5	6
0.715	100	5.197	5.222	5.128	4.50	5.12	4.468
0.715	200	7.247	7.213	7.420	6.37	7.30	7.129
1.	300	10.042	9.744	-	-	-	10.055

Table 1. Mean Nusselt number results (1 . . . 6 are related to results reported by: 1. Churchill *et al.*, (1977); 2. Hilpert, (1933); 3. Lange *et al.*, (1998); 4. Zhukauskas, (1972); 5. Wang and Trávníček, (2001); 6. Hoffmann, (2007)).

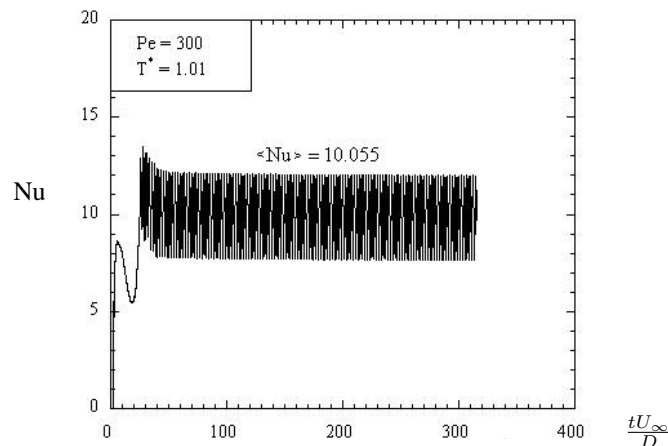


Figure 2. Time series of Nusselt number for a fluid flow around a single cylinder at $Pe = 300$.

4. RESULTS

In this work, six configurations are retained depending on the angle of rotation of the cylinders arrangement (Fig. 1): one cylinder upstream and two cylinders aligned vertically downstream (corresponding to $\alpha = 0^\circ = 120^\circ$), two cylinders aligned vertically upstream and a third cylinder downstream ($\alpha = 60^\circ$), and intermediate configurations ($\alpha =$

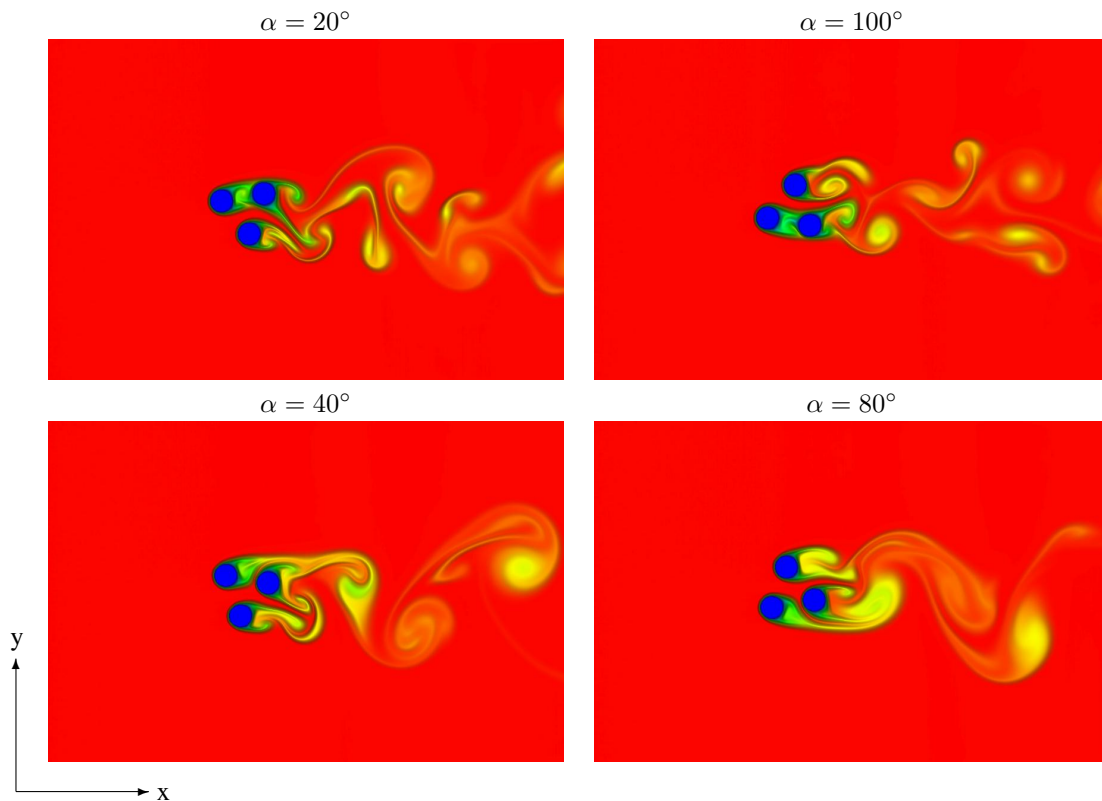


Figure 3. Sample of instantaneous temperature fields for $\alpha = 20^\circ, 40^\circ, 80^\circ$ and 100° .

$20^\circ, 40^\circ, 80^\circ, 100^\circ$). The distance between the cylinders is kept constant for all the configurations, equal to $2D$. The computational domain $(Lx, Ly) = (24D, 18D)$ is discretized on a Cartesian grid of $\Delta x = \Delta y = D/32$ mesh nodes, while the centre of the arrangement is located at $(x_c, y_c) = (9.1547D, 9D)$. The cylinders are numbered in the following way: for the first configuration corresponding to $\alpha = 0^\circ = 120^\circ$, the upstream cylinder is named cylinder 1, while the downstream cylinders are cylinder 2 (up) and 3 (down). Numerical results for the six configurations were obtained for a Reynolds number of $Re = 300$, Prandtl number, $Pr = 1$ and computational time of $T = 380D/U_\infty$.

In Eqs. (5-6), the constants α_f and α_θ are $-4000(\frac{U_\infty}{D})^2$, while β_f and β_θ are $-60(\frac{U_\infty}{D})$. The immersed boundary method induces a restriction in the computational time step, which is finally equal to $0.009525(\frac{D}{U_\infty})$.

4.1 Instantaneous visualization

The wake vortex dynamics, corresponding to configurations associated with the angle of rotation of the arrangement α , may be analysed in a comparative way through instantaneous visualizations of the temperature field. As it may be expected, the choice of α deeply determines the wake dynamics pattern. Fig. 3 shows the temperature field at the end of the numerical simulation for the configurations corresponding to $\alpha = 20^\circ, 40^\circ, 80^\circ$ and 100° . Very similar patterns are found in the experiences done by Lam and Cheung (1988).

For symmetry considerations (with respect to $y = 0$), results for $\alpha = 20^\circ$ may be compared with the case for $\alpha = 100^\circ$, while $\alpha = 40^\circ$ should be compared with $\alpha = 80^\circ$. For these cases, the interaction among the cylinders seems to be intensive, resulting in a far wake field which is highly influenced by the angle of rotation.

For the cases $\alpha = 20^\circ$ and 100° , the upstream cylinder's wake covers completely one of the downstream cylinders (see Fig. 3) resulting in a wake that is controlled by two vortex shedding: one corresponding to the pair of cylinders aligned streamwise and the other corresponding to the other cylinder. For intermediate configurations ($\alpha = 40^\circ$ and 80°) where there are semi-aligned cylinders, three wakes can be identified, corresponding to a triple vortex shedding. The interaction among cylinders results in a single well defined wake further downstream compared to $\alpha = 20^\circ$ and 100° . As it was expected, the temperature field for $\alpha = 80^\circ$ and $\alpha = 100^\circ$ has a symmetric behaviour when compared to the configurations for $\alpha = 40^\circ$ and $\alpha = 20^\circ$, respectively.

In configurations where at least two cylinders are vertically aligned, secondary flow is induced between them. This secondary flow, similar to a jet, changes its direction from upward to downward and vice-versa. This behaviour, often called bi-stable, which has been previously observed in the isothermal numerical simulations of fluid flow around two cylinders in side-by-side configuration (Ribeiro *et al.*, 2002), is found for $\alpha = 0^\circ$. Fig. 4 clearly shows this secondary flow for two characteristic times; while for $t = 295.26D/U_\infty$ the jet points downward, later for $t = 371.48D/U_\infty$ it

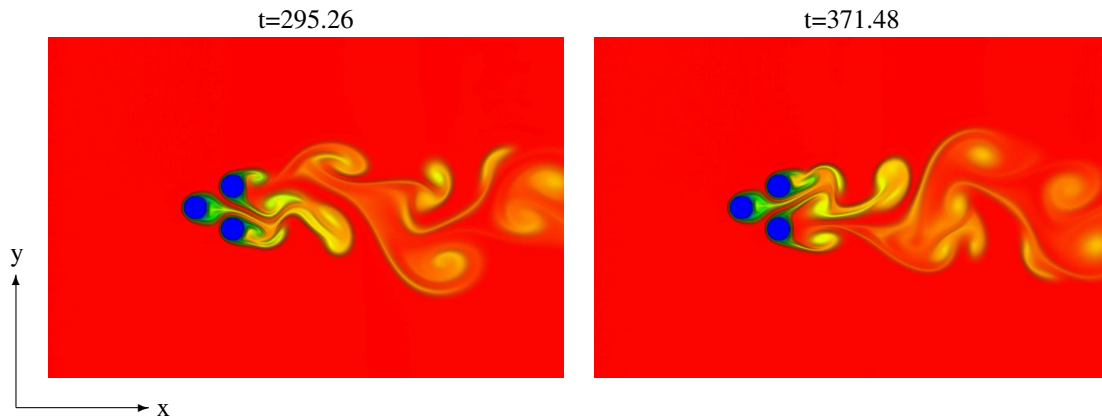


Figure 4. Temperature fields and vortex shedding at two different times in configuration $\alpha = 0^\circ$.

turns upward. The flapping behaviour of the jet seems to be related to the formation of a recirculation bubble from the upstream cylinder, which should accelerate between the two downstream cylinders. This bi-stable characteristic was also observed in the Lam and Cheung (1988) visualizations for gaps ratio lower than 2.29.

It is important to note that the jet flow between two cylinders is also observed in the other studied configurations (Fig. 3). However, in these cases, the jet is related to the vortex shedding produced by an upstream cylinder, a phenomenon that doesn't happen for the $\alpha = 0^\circ$ configuration, where there is no vortex shedding for the upstream cylinder.

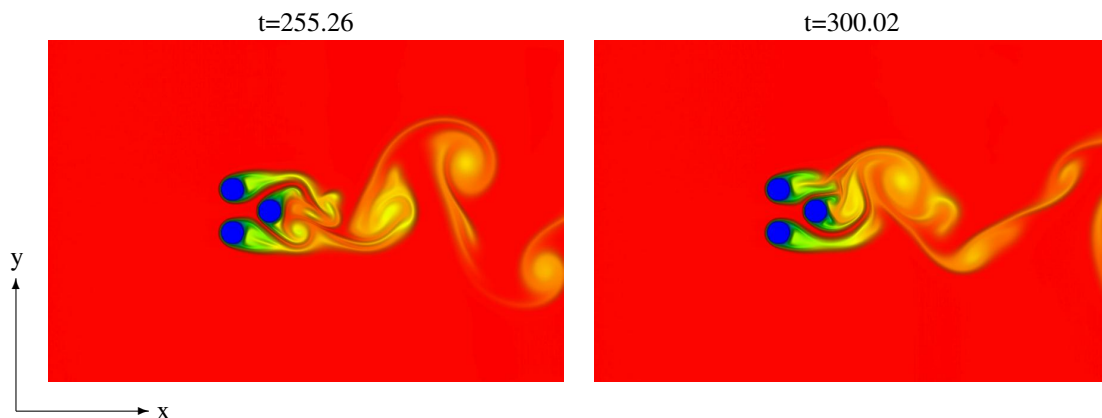


Figure 5. Temperature fields and vortex shedding at two different times for the configuration corresponding to $\alpha = 60^\circ$.

Fig. 5 illustrates the resulting vortex shedding for the configuration corresponding to $\alpha = 60^\circ$ at two characteristic times. In this case, the jet between the two upstream cylinders directly impacts on the downstream cylinder while being deviated upward and downward, driven by the periodical vortex shedding of the upstream cylinders. Intense recirculation is observed on the downstream cylinder while, as for cases with $\alpha = 40^\circ, 80^\circ$, a single wake is formed further downstream.

4.2 Statistical analysis for C_D, C_L and Nu

Time series of drag and lift coefficients and Nusselt numbers are computed for each cylinder and for the global configuration, using the control-volume method. Time series of drag coefficient and Nusselt number are shown in Fig. 6, for $\alpha = 100^\circ$. The secondary flow, already observed in the visualizations, leaves its signature on the C_D and C_L values. For the configuration with $\alpha = 0^\circ$, for example, the secondary flow induces a higher oscillation amplitude on the two downstream cylinders, denoted by the augmentation of root mean square (rms) values of drag and lift coefficient ($C_{D_{rms}}, C_{L_{rms}}$). In this configuration, and also for $\alpha = 60^\circ$, the mean lift coefficients of the two vertically aligned cylinders have the same magnitude but opposite directions, resulting on a repulsion between the cylinders. Table 2 summarizes the statistic results for mean and rms values for $\alpha = 0^\circ$.

	C_{D_m}	$C_{D_{rms}}$	C_{L_m}	$C_{L_{rms}}$	Nu_m	Nu_{rms}
Cylinder 1	1.018	0.064	-0.001	0.057	4.944	1.473
Cylinder 2	1.343	0.219	-0.135	0.521	2.871	2.938
Cylinder 3	1.270	0.213	0.169	0.469	2.983	2.717
Global	3.659	0.269	0.039	0.682	4.952	1.473

Table 2. Statistical results for drag and lift coefficients and Nusselt number for $\alpha = 0^\circ$.

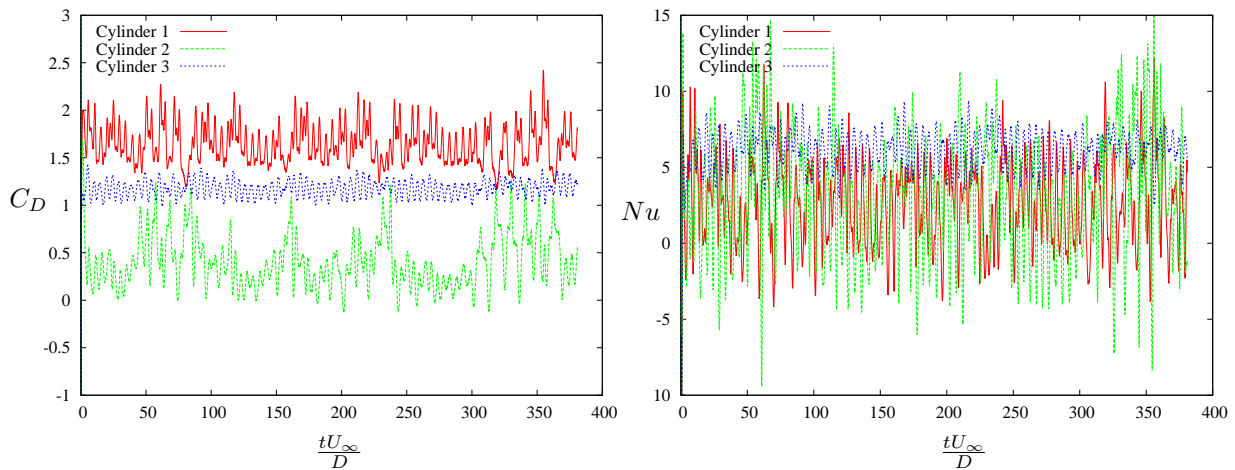


Figure 6. Time series of drag coefficient and Nusselt number for $\alpha = 100^\circ$.

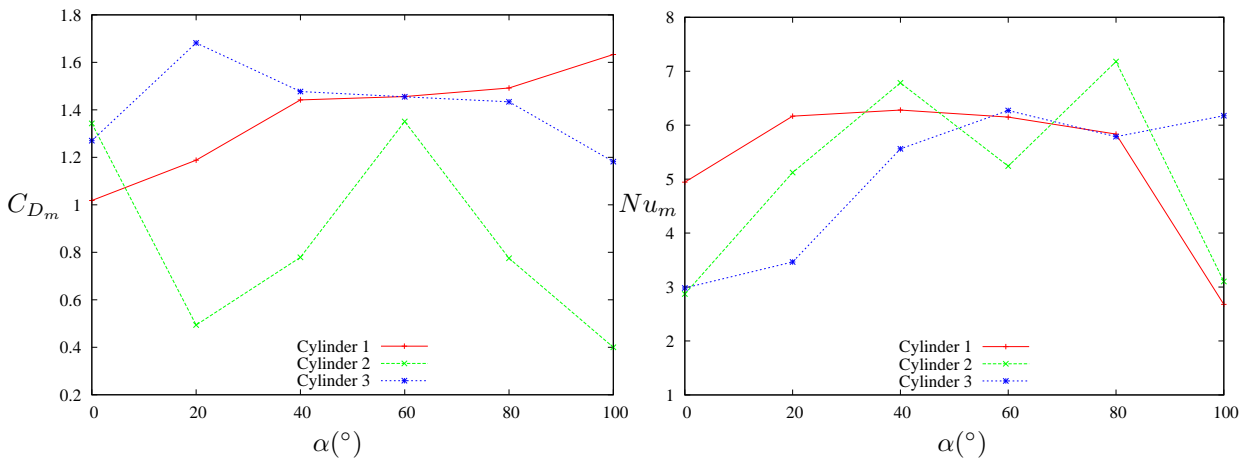


Figure 7. Mean drag coefficients (left) and Nusselt numbers (right) of the three cylinders related to configuration angle.

Arrangements with $\alpha = 20^\circ$ and $\alpha = 100^\circ$ have approximately the same behaviour in terms of drag coefficients. This is a result of the symmetry that exists between the two configurations in relation to the $y = 0$ plane. Both configurations show downstream cylinders completely inside the wake generated by an upstream cylinder, which decreases substantially the value of downstream cylinder's drag coefficient. Differences can be found in terms of mean lift coefficient. While for $\alpha = 20^\circ$ the secondary flow is driving upward (which implies in a positive mean lift coefficient for all the cylinders), for $\alpha = 100^\circ$ the secondary flow has an opposite effect.

For configurations corresponding to $\alpha = 40^\circ$ and $\alpha = 80^\circ$ similar trends are found. However, for these cases two cylinders are being driven upward ($\alpha = 40^\circ$) or downward ($\alpha = 80^\circ$) depending on the direction of the secondary flow. As the downstream cylinder is not completely inside the upstream cylinder's wake, the value of its mean drag coefficient is not so low as it was for the $\alpha = 20^\circ$ and $\alpha = 100^\circ$ cases.

Fig. 7 presents the mean drag coefficients and the Nusselt numbers of the three cylinders for all considered configurations. The mean drag coefficients of cylinders 1 and 3 have an opposite behaviour when α is modified. From Fig. 7 it can be seen that these two cylinders have opposite values in symmetrical configurations, e.g. $C_{D_m}^1$ (mean drag coefficient for cylinder 1) at $\alpha = 20^\circ$ equals $C_{D_m}^3$ at $\alpha = 100^\circ$. Due to the symmetry, cylinder 1, for the configuration with $\alpha = 100^\circ$, has an effect on the flow similar to the one exerted by cylinder 3 when $\alpha = 20^\circ$.

When $\alpha = 60^\circ$, the two upstream cylinders have approximately the same mean drag coefficient because they are vertically aligned, which also happens for cylinders 2 and 3 in the first configuration ($\alpha = 0^\circ$). The aerodynamic coefficients of cylinders 1 and 3 have less variation compared to cylinder 2, for the different angles of attack. Cylinder 2 is highly influenced by the upstream cylinder wake in the $\alpha = 20^\circ$ and $\alpha = 100^\circ$, resulting in a significant drag reduction. For $\alpha = 40^\circ$ and $\alpha = 80^\circ$ a reduction is also noticed in the figure but not with the same magnitude, because cylinder 2 is not completely inside the upstream cylinder wake.

Fig. 7 also shows the mean Nusselt number variation of the three cylinders for different configurations. In the first configuration, $\alpha = 0^\circ$, cylinders 2 and 3 have approximately the same Nusselt numbers because they are vertically aligned. This also happens with cylinders 1 and 3 at $\alpha = 60^\circ$. The highest Nusselt numbers are found at $\alpha = 40^\circ$ and $\alpha = 80^\circ$, both for cylinder 2. This means that a cylinder partially positioned inside an upstream cylinder wake has its own

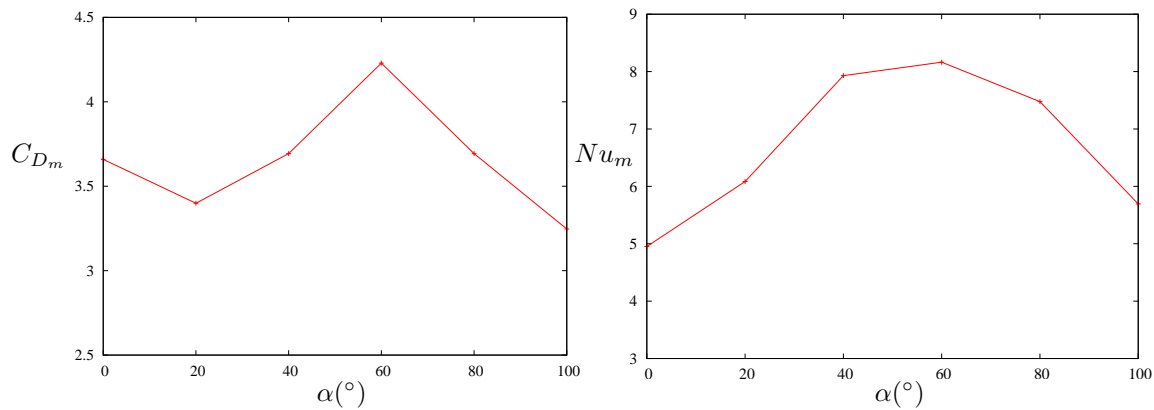


Figure 8. Global drag coefficients (left) and Nusselt numbers (right) of the three cylinders related to configuration angle.

	$\alpha = 0^\circ$	$\alpha = 20^\circ$	$\alpha = 40^\circ$	$\alpha = 60^\circ$	$\alpha = 80^\circ$	$\alpha = 100^\circ$
St	0.089	0.203	0.109	0.090	0.103	0.212

Table 3. Strouhal numbers for different configurations.

convective heat transfer coefficient enhanced due to the higher turbulence generated.

The global analysis of mean drag coefficient and Nusselt number is shown in Fig. 8. For the drag coefficient, the global mean value may be related to the friction factor thus it may be useful for pressure losses calculations. Clearly, the configuration $\alpha = 60^\circ$ is the one with the highest mean global drag coefficient. The arrangements with symmetry related to $y = 0$ have the same global drag coefficient.

As expected, the highest Nusselt number is found in the $\alpha = 60^\circ$ configuration. This indicates a direct relation between the Nusselt number and the drag coefficient, which is also at its maximum in this configuration. It is also noticed that the pairs of symmetrical configurations ($\alpha = 20^\circ, 100^\circ$ and $\alpha = 40^\circ, 80^\circ$) have approximately the same Nusselt numbers, while the cylinders arrangement with $\alpha = 0^\circ$ presents the lowest convective heat transfer coefficient.

4.3 Frequency analysis

Time series for the velocity components were recorded at different positions on the wake of the arrangement for frequency analysis purposes. Each x -plane located at $x = 2D, 3D$ and $4D$ from $x = x_c$, has three vertical points corresponding to $y = y_c, y_c - 1.5D, y_c + 1.5D$, respectively. Time series of vertical velocity at $x = x_c + 4D$, for the three vertical positions, were used to analyse the spectral characteristics of the wakes for the different arrangements.

Fig. 9 presents the power density spectra for all the configurations. This figure confirms the similarity of the three pairs of symmetrical configurations regarding the frequency corresponding to peak values. These values are very close between the configurations pairs $\alpha = 0^\circ, 60^\circ, \alpha = 20^\circ, 100^\circ$ and $\alpha = 40^\circ, 80^\circ$. Table 3 summarises the Strouhal numbers corresponding to peak values of kinetic energy. Lam and Cheung (1988) found Strouhal number of 0.1 for $\alpha = 0^\circ$ for a rather high Reynolds number.

Regarding the composition of the spectra for different arrangements, they do not follow symmetrical considerations. As it was seen in the instantaneous visualizations, configurations associated with $\alpha = 40^\circ, 60^\circ$ and 80° , show a well defined single wake further downstream. This resulting flow dynamics are quantitatively confirmed by spectra where great part of the kinetic energy is concentrated around the peak values. Different spectra are observed for the cases corresponding to $\alpha = 0^\circ, 20^\circ$ and 100° . As also shown, these configurations produce a highly perturbed far field wake, which reflects in a spectra where the kinetic energy is extended for a largest range of frequencies.

4.4 Mean and turbulent profiles

Data recorded at the three transversal planes mentioned above was used to compute mean and turbulent statistics. Fig 10 shows mean profiles for the configurations corresponding to $\alpha = 60^\circ$ and $\alpha = 40^\circ$. The mean streamwise and vertical velocities, as well as the mean temperature profiles, are highly influenced by the arrangement of the cylinders. This influence becomes less significant as the flow moves away from the cylinders. Symmetric arrangements, such as $\alpha = 60^\circ$, result in symmetrical temperature and longitudinal velocity profiles.

In configurations where a downstream cylinder is completely or partially covered by an upstream cylinder wake, the variation of the temperature and velocity fields is more significant, as shown in Fig. 10 for $\alpha = 40^\circ$. Negative peaks in the streamwise velocities indicate recirculation and are observed in regions close to the cylinders. Fig. 10 also shows that negative velocities denoting recirculation processes are more intense (unless for $x \geq x_c + 2D$) in non-symmetrical

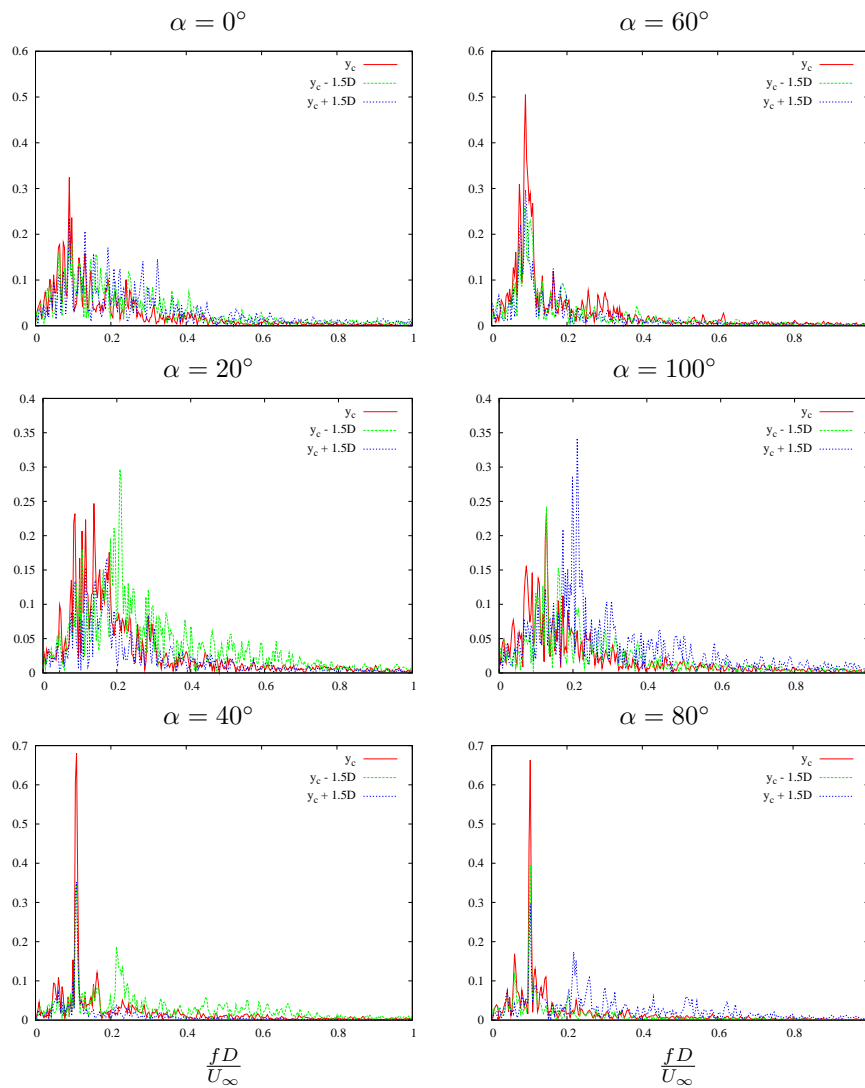


Figure 9. Power density spectra for vertical velocity at $x = x_c + 4D$ and $y = y_c$ (red), $y_c - 1.5D$ (green), and $y_c + 1.5D$ (blue) for all configurations.

arrangements like $\alpha = 40^\circ$ that in symmetrical configurations such as $\alpha = 60^\circ$.

Vertical profiles of normal and shear Reynolds stress in the three streamwise locations are shown in Fig. 11 for $\alpha = 60^\circ$ and $\alpha = 40^\circ$. Considerations about the symmetry/asymmetry of the arrangements configurations, results also on symmetrical/asymmetrical vertical profiles for the turbulent quantities. As the Fig. 11 shows, the normal and shear stress profiles for $\alpha = 60^\circ$ have maxima values nearly 50% higher than the ones for $\alpha = 40^\circ$ configuration. This large difference is directly related with the configuration arrangement and results in a considerable increase of mixing and heat transfer, as was denoted by the Nusselt number results for global configurations (Fig. 8).

5. Conclusions

In this work the fluid flow and heat transfer around an arrangement of three cylinders was studied using two-dimensional direct numerical simulation. Results were obtained for different configurations of the arrangement, depending on the characteristic angle α . For all configurations, a secondary flow induced by the cylinders contributes significantly to the vortex shedding mechanism. When $\alpha = 0^\circ$, the secondary flow changes its direction from upward to downward and vice-versa, a behaviour often called bi-stable. For configurations corresponding to $\alpha = 40, 60, 80^\circ$, a well defined single wake may be found further downstream. Other arrangements produced a highly perturbed wake. This may be clearly seen in the instantaneous visualizations and specifically in the frequency analysis.

Time series of drag and lift coefficients and Nusselt numbers were computed for each cylinder and for the global configuration. Arrangements with $\alpha = 20^\circ$ and $\alpha = 100^\circ$ have nearly the same behaviour in terms of drag coefficients. This is a result of the symmetry, in relation to the $y = 0$ plane, that exists between the two configurations. When $\alpha = 0^\circ$, the secondary flow induces a higher oscillation amplitude on the two downstream cylinders, described by the increase of root mean square (rms) values of drag and lift coefficient ($C_{D_{rms}}, C_{L_{rms}}$). The global analysis of mean drag coefficient

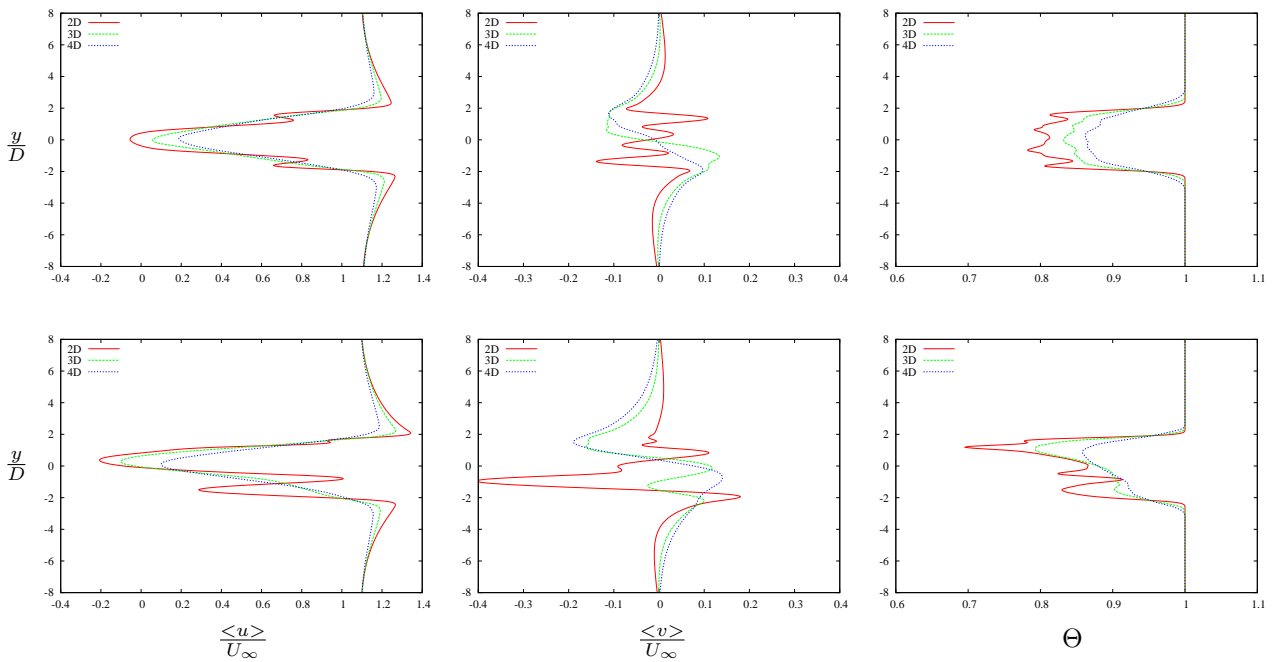


Figure 10. Mean streamwise (left) and vertical (middle) velocities and temperature (right) profiles for $x = 2D, 3D, 4D$ from the arrangement centre x_c for $\alpha = 60^\circ$ (top) and $\alpha = 40^\circ$ (bottom).

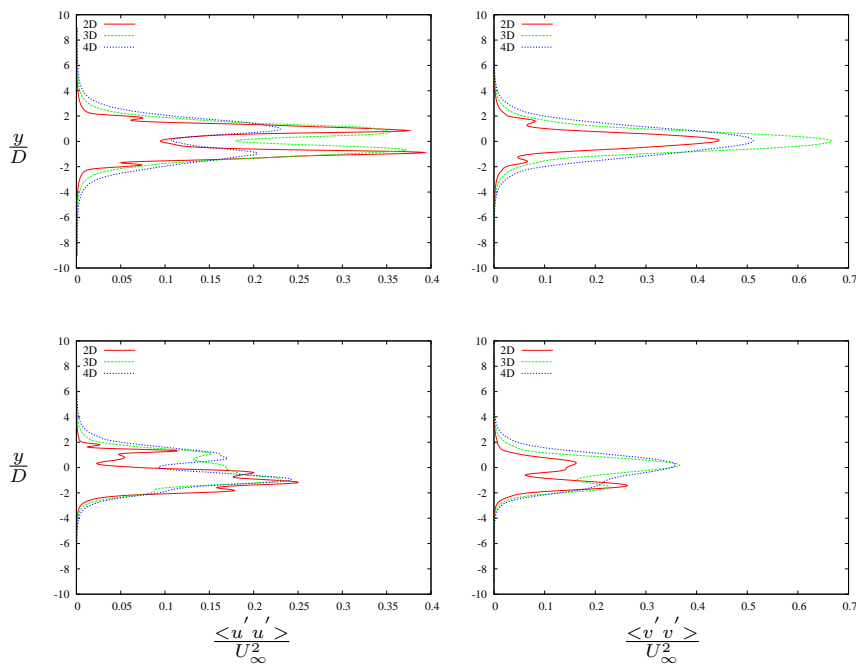


Figure 11. Normal (left) and vertical (right) Reynolds stress profiles for $x = 2D, 3D, 4D$ from the arrangement centre x_c for $\alpha = 60^\circ$ (top) and $\alpha = 40^\circ$ (bottom).

and Nusselt number show maxima values for $\alpha = 60^\circ$, while the lowest convective heat transfer coefficient is obtained for $\alpha = 0^\circ$.

Spectral analysis from time series of vertical velocities, recorded at different x -locations, indicate that, depending on the arrangement, different Strouhal numbers corresponding to peak values of kinetic energy may be found. The distribution of spectra is also influenced by the configuration of the arrangement. Finally, mean and turbulent profiles are shown for two configurations, $\alpha = 60^\circ$ and $\alpha = 40^\circ$. Maxima values for Reynolds stress denote an intense mixing processes that enhances the heat transfer for $\alpha = 60^\circ$.

6. ACKNOWLEDGEMENTS

The authors would like to acknowledge the CNPq (Conselho Nacional de Desenvolvimento Científico e Tecnológico) for the PIBIC fellowships for this research.

7. REFERENCES

- Bearman, P.W. and Wadcock, A.J., 1973, "The interaction between a pair of circular cylinders normal to a stream", *J. Fluid Mech.*, Vol.61, pp. 499-511.
- Chou, J.H. and Chao, S.Y., 1991, "The flow interaction among three circular cylinders", *The Chinese Journal of Mechanics*, Vol.7, pp. 163-9.
- Churchill, S.W. and Bernstein, M., 1977, "A Correlation Equation for Forced Convection from Gases and Liquids to a Circular Cylinder in Cross Flow", *J. Heat Transfer*, Vol.99, pp. 300-306.
- Giacomello, M.V., Rocha, L.A.O., Schettini, E.B.C. and Silvestrini, J.H., 2006, "Simulação numérica de escoamentos ao redor de cilindros com transferência de calor", 5ª Escola de primavera de transição e turbulência, Rio de Janeiro, Brasil.
- Goldstein, D., Handler, R. and Sirovich, L., 1993, "Modeling a no-slip boundary condition with an external force field", *J. Comp. Phys.*, Vol.105, pp. 354-366.
- Hilpert R., 1933, "Wümrmeabgabe von geheizten Drähten und Röhren im Luftstrom", *Forsch. Geb. IngWes.*, Vol.4, pp. 215-224.
- Hoffmann, A.M., 2007, "Estudo do escoamento ao redor de dois cilindros equidistantes com transferência de calor por simulação numérica", Salão de iniciação científica PUCRS, Porto Alegre, Brasil.
- Igarashi, T., 1993, "Aerodynamic forces acting on three circular cylinders having different diameters closely arranged in line", *J. Wind Eng. Industrial Aerodynamics*, Vol.49, pp. 369-78.
- Lam, K. and Zou, L., 2009, "Experimental study and large eddy simulation for the turbulent flow around four cylinders in an in-line square configuration", *Int. J. Heat and Fluid Flow*, Vol.30, pp. 276-285.
- Lam, K. and Cheung W.C., 1988, "Phenomena of vortex shedding and flow interference of three cylinders in different equilateral arrangements", *J. Fluid Mech.*, Vol.196, pp. 1-26.
- Lamballais, E. and Silvestrini, J.H., 2002, "Direct numerical simulation of interactions between a mixing layer and a wake", *Journal of Turbulence*, Vol.3, No. 28, pp. 1-21.
- Lange, C. F., 1998, "Momentum and heat transfer from cylinders in laminar crossflow at $10 - 4 \leq Re \leq 200$ ", *Int. J. Heat Mass Transfer*, Vol.41, No.22, pp. 3409-3430.
- Lardeau, S., Lamballais, E. and Bonnet J.P., 2002, "Direct numerical simulation of a jet controlled by fluid injection", *J. turbulence*, Vol.3, 002.
- Linnick, M. and Fasel, H., 2003, "A high-order immersed boundary method for unsteady incompressible flow calculations", *Proceedings of 16th AIAA Computational Fluid Dynamics Conference*, p. 1124.
- Ortega, M.A., Girardi, R.M. and Silvestrini, J.H., 2007, "The formation region behind a blunt body fitted with splitter plattes", 45th AIAA Aerospace Sciences Meeting and Exhibit, Reno, Nevada.
- Polak, D. R., and Weaver, D. S., 1995, "Vortex shedding in normal triangular tube arrays", *Journal of Fluids and Structures*, Vol.9, pp. 1-17.
- Ribeiro, P.A.R., Schettini E.B.C. and Silvestrini, J.H., 2004, "Bluff-bodies vortex shedding supression by direct numerical simulation", *Thermal Engineering*, No.5, pp. 3-8.
- Ribeiro, P.A.R., Souza, T.F. and Silvestrini, J.H., 2002, "Análise do desprendimento de vórtices de dois cilindros perpendiculares ao escoamento por simulação numérica direta", Escola de transição e turbulência, Florianópolis, Brasil.
- Vitola, M.A., Schettini, E.B.C. and Silvestrini, J.H., 2004, "Uniform shear flow around a circular cylinder at a sub-critical reynolds number", *Proceedings of the 10th Brazilian Congress of Thermal Sciences and Engineering*, Rio da Janeiro, Brazil.
- Wang, A.-B. and Trávníček, Z., 2001, "On the linear heat transfer correlation of a heated circular cylinder in laminar crossflow using a new representative temperature concept", *Int. J. Heat Mass Transfer*, Vol.44, No.24, pp. 4635-4647.
- Wang, Z.J. and Zhou, Y., 2004, "Vortex interactions in a two side-by-side cylinder near-wake", *Int. J. Heat Fluid Flow*, Vol. 26, pp. 362-377.
- Williamson, C.H.K., 1985, "Evolution of a single wake behind a pair o bluff bodies", *J. Fluid Mech.*, Vol.159, pp. 1-18.
- Williamson, C.H.K., 1996, "Vortex dynamics in the cylinder wake", *Annual Review in Fluid Mechanics*, Vol.28, pp. 477-539.
- Wu, H.-W., Perng S.-W., Huang, S.-Y. and Jue, T.-C., 2006, "Transient mixed convective heat transfer predictions around three heated cylinders in a horizontal channel", *Int. J. Numerical Methods for Heat and Fluid Flow*, Vol.16, No. 6, pp. 674-692.
- Zhukauskas, A., 1972 "Heat Transfer from Tubes in Crossflow", *Advances in Heat Transfer*, Vol.8, pp. 93-160.

8. Responsibility notice

The author(s) is (are) the only responsible for the printed material included in this paper